Chapter 4

Experimental Setup

In this chapter, the experimental setup utilized for measuring the reaction kinetics and fs-dynamics of small noble metal clusters will be presented. The description will begin with the triple quadrupole mass spectrometer, which is used for cluster production and analysis followed by a detailed presentation of the octopole ion trap. The measurement procedure for the study of the cluster reactivity will be outlined. Afterwards, the focus will be set on the description of the laser system, where the generation and characterization of the fs-laser pulses will be presented. The pump-probe setup as well as the measurement procedure employed for the investigation of the clusters dynamics on ultrashort time scale will be described.

4.1 Cluster Production and Analysis

In order to study the chemical reactions of cluster ions with molecules in the gas-phase, a large variety of experimental techniques have been developed. A key aspect which differentiates between various experimental setups is given by the conditions under which the chemical reaction is carried out. In the following, an overview of the different techniques commonly used to investigate the chemical reactions of cluster ions is presented.

In the simplest case, the chemical reaction can take place during the cluster formation process. In this scenario, the reactive gas is introduced into the cluster source together with the carrier gas (helium or argon).[80,81] Since this procedure does not

provide well defined reaction conditions, other techniques like flow tube reactors and ion traps are commonly used since they separate the cluster formation process and the chemical reaction.

The *flow tube reactor* is a widely used experimental approach for the investigation of ion-molecule reactions. After the production of a cluster beam by using different types of cluster sources (laser vaporization source,[82] gas aggregation source,[83] ion sputtering source[84] etc.), the ions are guided inside a flow tube reactor where a mixture of reactive and buffer gas is introduced. During their flight through the reactor tube which is usually over 1 m long, the clusters can react with the respective gas mixture and the reaction products are extracted and analyzed by means of mass spectrometry.[32,85] This method allows for the investigation of chemical reactions over a wide range of the reactive gas pressure.

Another experimental approach is to store the cluster ions inside traps (magnetic traps,[86,87] radio frequency traps[88–90]), where they are exposed to the reactive gases. An example of this technique is the *Fourier Transform Ion Cyclotron Resonance* method (FT-ICR), where a strong magnetic field is used for storing the ions up to several seconds and the mass spectra of the reaction products are obtained using Fourier transform methods.[86] The major disadvantage lies in the very low pressure range of the reactant gas that is accessible with this technique (up to 10^{-5} $mbar$). The *Penning trap*[87] relies on the same storage principle and is commonly used in combination with a time-of-flight (TOF) mass spectrometer. *Radio frequency* (RF) ion traps or multipole ion traps employ the principle of storing ions by applying an inhomogeneous RF-field combined with a DC-field on the metal rods of the trap. As the number of rods (poles) increases, the potential is steeper and the field free region inside the trap is larger. Therefore quadrupole, octopole, hexadecapole or even 22-pole RF-ion traps, are intensively used for the investigation of chemical reactions in the gas-phase.[88,89] Usually, these types of ion traps are inserted into a tandem mass spectrometer which allows the mass selection of the clusters prior to entering the trap as well as the mass analysis of the reaction products.

In the experiments presented in this work, an octopole ion trap coupled with a triple quadrupole mass spectrometer is utilized. A detailed description of the experimental setup for the cluster production, analysis and the measurement procedure will be presented in the following subsections.

4.1.1 Triple Quadrupole Mass Spectrometer

A detailed view of the experimental setup is presented in Fig. 4.1. The clusters are produced by an ion sputtering source (CORDIS - cold reflex discharge ion source[84]), directed into the triple quadrupole system and guided into the octopole ion trap where chemical reactions are carried out. The reaction products are extracted and mass analyzed with the last quadrupole and monitored with a channeltron detector.

The principle of the cluster source relies on the ionization of a rare gas (xenon or argon) and the subsequent extraction of four highly energetic ion beams. An enlarged view of the cluster source and target chamber is presented in Fig. 4.2. The cathode of the source (six tantalum filaments supported on a tantalum holder) is electrically heated (180 A, 6 V) and emits electrons which are accelerated under a DC-field (60 V). The accelerated electrons ionize the rare gas atoms ($p_{Xe} = 6 \cdot 10^{-2}$ $mbar$) and consequently, a plasma is obtained. The plasma is kept in the center of the chamber with a strong magnetic field produced by 18 $Co-Sm$ permanent magnets. By using three electrostatic lenses with a high positive (10 kV), negative (-3 kV) and ground potential, four highly energetic ion beams are extracted and directed onto the metal targets. The clusters (neutral, positive and negative) are sputtered off from the targets and the charged species are extracted into the first quadrupole Q_0 by using four electrostatic lenses. Due to the high applied currents and voltages, as well as the high thermal energy released during the sputtering process, the source and the targets are continuously water-cooled. In order to enhance the production of anionic clusters, a cesium (Cs) oven was introduced inside the target chamber.[75] Since Cs atoms have a very low electron affinity[a] ($E_{EA} = 0.47$ eV[91]), an electron can be easily transferred to the neutral clusters through collisions. The evaporation of Cs atoms inside the target chamber leads to a significant increase in the yield of negatively charged clusters.

The generation of a continuous cluster signal and the relatively high intensities of the cluster current (a few nA for the cations and up to 1 nA for the anions) are the most important advantages of this cluster source. On the other hand, the exponential decrease of the signal intensity with increasing cluster size makes this source suitable

[a]The electron affinity (EA) is defined as the energy corresponding to the transition from the electronic ground state of an anionic molecule (vibrational ground state of the anion $\nu(X^-) = 0$) into the electronic ground state of the neutral molecule (vibrational ground state of the neutral $\nu(X) = 0$).

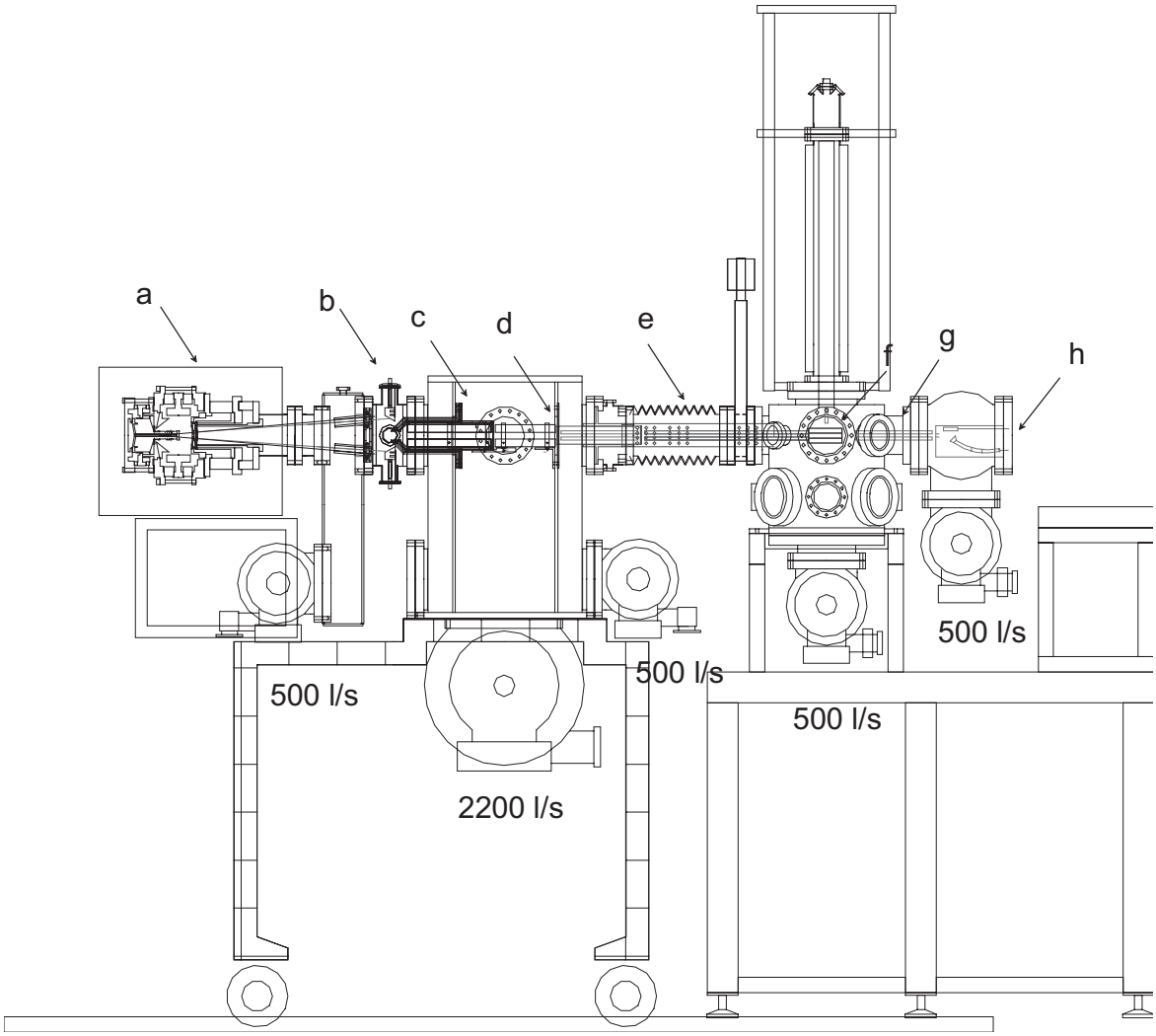

Figure 4.1: The experimental apparatus: cluster source, triple quadrupole mass spectrometer, detector. (a) cluster source (CORDIS), (b) target chamber, (c) Q_0 quadrupole, (d) Q_1 quadrupole (mass filter), (e) Q_2 quadrupole (guiding quadrupole), (f) octopole ion trap, (g) Q_3 quadrupole mass spectrometer, (h) channeltron detector. The high-vacuum conditions are ensured by using four turbo-pumps with a pumping capacity of 500 l/s and one turbo-pump with a capacity of 2200 l/s.

only for the investigation of small clusters (up to $10 - 20$ atoms/cluster).

The highly energetic clusters enter the first guiding quadrupole Q_0, which is filled with helium as buffer gas. They are thermalized and collimated on the axis of the quadrupole through collisions with the buffer gas molecules. Q_0 is a home-built sys-

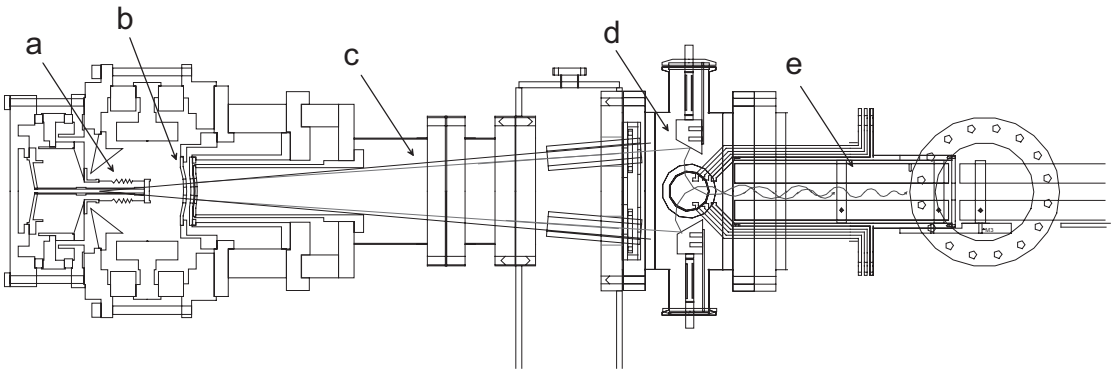

Figure 4.2: The cluster source, target chamber and Q_0 quadrupole: (a) tantalum filaments, (b) extraction system composed of three electrostatic lenses, (c) four highly energetic xenon ion beams, (d) targets, (e) Q_0 quadrupole ("phase-space compressor").

tem[92] and produces an increase of the cluster signal transmission by a factor of 100. Since this quadrupole reduces the volume in the phase-space, Q_0 is referred to as "phase-space compressor". The thermalized clusters are then transferred into the second quadrupole Q_1, where the mass selection is performed. After mass selection, the beam is guided into the third quadrupole Q_2 where the clusters can be further thermalized by collisions with helium as buffer gas and a very narrow kinetic energy distribution of the cluster beam can be obtained. A typical example of the cluster signal as a function of the retarding potential, with or without introducing helium in Q_2 is presented in Fig. 4.3, where the grey line represents the kinetic energy distribution of the cluster beam. Comparing Fig. 4.3 (a) to Fig. 4.3 (b), it can be clearly seen that the kinetic energy distribution of the cluster beam is significantly reduced when helium is introduced inside Q_2.

The lowering of the kinetic energy distribution of the clusters in Q_2 can also be utilized in other experiments such as two-photon photoemission on deposited silver clusters.[93] In these experiments, Q_2 has been used for achieving the "softlanding" of the clusters on highly oriented pyrolytic graphite (HOPG) surfaces, *i.e.* the clusters were deposited with a kinetic energy of about 1 eV/cluster, which allows for a fragmentation-free deposition of the clusters.

The clusters are then transferred inside the "heart" of the experimental setup, namely the octopole ion trap, where a mixture of buffer gas (helium or argon)[b] and

[b]For the reactivity measurements of the Au_n clusters towards oxygen and carbon monoxide only

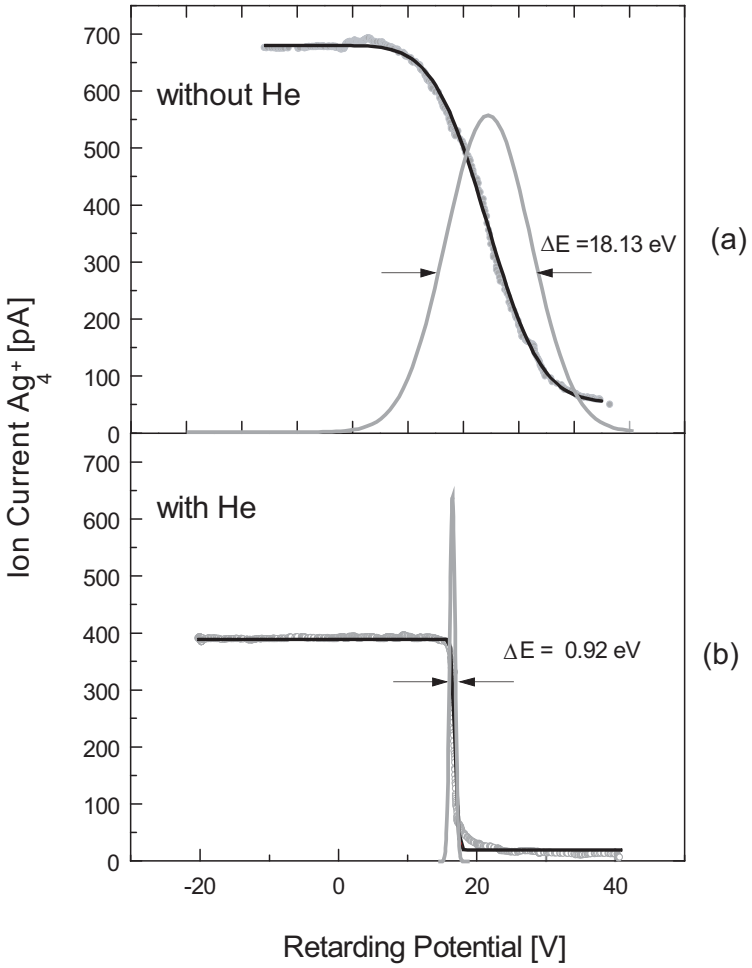

Figure 4.3: Softlanding: reduction of the kinetic energy distribution of clusters inside Q_2 by means of helium collision. The cluster signal intensity (black line) and kinetic energy distribution, which is given by the first derivative of the ion signal (grey line) of the cluster beam is shown as a function of the retarding potential applied on the sample without introducing helium inside Q_2 (a) and in the presence of helium inside Q_2 (b). There is a significant change in the cluster kinetic energy distribution from a FWHM of 18.13 eV without helium to a FWHM of 0.92 eV in the presence of helium inside Q_2.

reactive gas is introduced. The octopole is connected with a helium cryostat and a minimum temperature of about 20 K can be reached inside the trap. Due to the complexity and importance of the octopole ion trap, a detailed description will be given

helium was used as buffer gas inside the octopole ion trap. Argon and helium were used in the case of experimental measurements on Ag_n clusters.

in the next subsection. The reaction products are extracted into the last quadrupole mass spectrometer Q_3 and the ions are recorded with a channeltron detector. The entire apparatus works under vacuum conditions and the base pressure is in the range of $10^{-7} - 10^{-8}$ $mbar$. The triple quadrupole setup (Q_1, Q_2, Q_3) is a commercially available system (Extrel, Model 150-QC).

4.1.2 Octopole Ion Trap

The method of guiding and trapping charged particles by time-dependent forces (radio frequency fields) started in the 1950's with the discovery of the quadrupole mass filter.[94–96] The working principle relies on the superposition of a RF-field and a DC-field. If one assumes that a charged particle moves in an electric field composed of a static and a time-dependent part, then the equation of motion is given by:

$$m\ddot{\overrightarrow{r}} = q\overrightarrow{E_0}(\overrightarrow{r})\cos\omega t + q\overrightarrow{E_s}(\overrightarrow{r}) \tag{4.1}$$

where $\overrightarrow{r}$ represents the coordinate vector of the charged particle, m and q represent the mass and the charge of the ion, $\overrightarrow{E_0}(\overrightarrow{r})$ is the RF-field amplitude, ω is the field frequency and $\overrightarrow{E_s}(\overrightarrow{r})$ represents the static field. The solution of this differential equation is a superposition of a smooth drift motion $\overrightarrow{R_0}(t)$ (guiding motion) and a rapidly oscillating motion $\overrightarrow{R_1}(t) \sim cos\omega t$ (wiggling motion).

$$\overrightarrow{r(t)} = \overrightarrow{R_0}(t) + \overrightarrow{R_1}(t) \tag{4.2}$$

An *effective potential* $V(\overrightarrow{R_0})$ can be introduced,

$$V(\overrightarrow{R_0}) = \frac{q^2\overrightarrow{E_0}^2}{4m\omega^2} + q\Phi_s \tag{4.3}$$

where Φ_s is the electrostatic potential defined as:

$$\overrightarrow{E_s} = -\nabla\Phi_s \tag{4.4}$$

Thus, the motion of a charged particle can be characterized in terms of the effective potential. For the particular case of a multipole field produced by $2n$ cylindrical metal electrodes ($n = 2,\ 3,\ 4,\ \cdots$) arranged in a circular geometry with the radius r_0, the expression of the effective potential becomes:[97]

$$V(\hat{r}) = \frac{n^2}{4}\ \frac{q^2}{m\omega^2}\ \frac{V_0^2}{r_0^2}\ \hat{r}^{2n-2} \tag{4.5}$$

where $\hat{r} = r/r_0$ is the reduced radial coordinate and V_0 is the amplitude of the RF-voltage. For the octopole ion trap employed in the experiments presented in this work, the effective potential has a value of approximately $V = 1.1\ eV$.[75] A comparison between the effective potential in the case of an octopole ($n = 4$) and a quadrupole ($n = 2$) is presented in Fig. 4.4 (a). From this picture, it can be clearly seen that the potential walls in the case of an octopole ($V \sim r^6$) are steeper than for a quadrupole ($V \sim r^2$). Moreover, the trapping region, *i.e.* the field-free region in the case of an octopole ion trap is larger than for the quadrupole.

An important issue for the ion motion in a variable electrical field is the stability of the ion trajectory. The total ion energy, composed of the energy in the guiding and wiggling motion should not be increased during the particle movement in the variable electrical field. Taking this condition into account, one can define the *adiabaticity parameter* η as:

$$\eta = \frac{2q\nabla E_0}{m\omega^2} \tag{4.6}$$

For stable ion trajectories[c] the adiabaticity parameter was empirically found to be $\eta \leq 0.3$.[97] For this value, the variable electrical field has no significant influence on the total ion energy. From equation 4.6, one can notice that for a given mass m, charge q and frequency ω, the adiabaticity parameter η depends only on the inhomogeneity of the field E_0. Fig. 4.4 (b) shows a typical trajectory of a charged particle inside an octopole ion trap calculated for an adiabaticity parameter of $\eta = 0.3$.

The temperature variable octopole ion trap utilized for the experiments presented in this work, was built by H. Heß.[75] The eight metal electrodes (74 mm long, 3 mm thick) are arranged in a circular geometry with a diameter of 13 mm. Two computer controlled electrostatic lenses (L_1 and L_2) mounted at the entrance and at the exit of the trap allow the operation of the trap in the filling, storing or extraction mode. The entire trap is introduced in a gold plated housing in order to avoid thermal losses and connected with a helium cryostat (APD Cryogenics Inc., Model HC-2D). By using a heating wire fixed on the connection between the trap and the cryostat, a control of the trap temperature in the range $20\ K - 300\ K$ can be achieved. A detailed view of the ion trap connected to the cryostat is given in Fig. 4.5. The temperature of the trap is monitored by two thermocouples (Gold/Iron and Chromel/Alumel) mounted

[c]The condition of stability of ion trajectories in a variable electrical field is usually referred to as "safe operation condition".

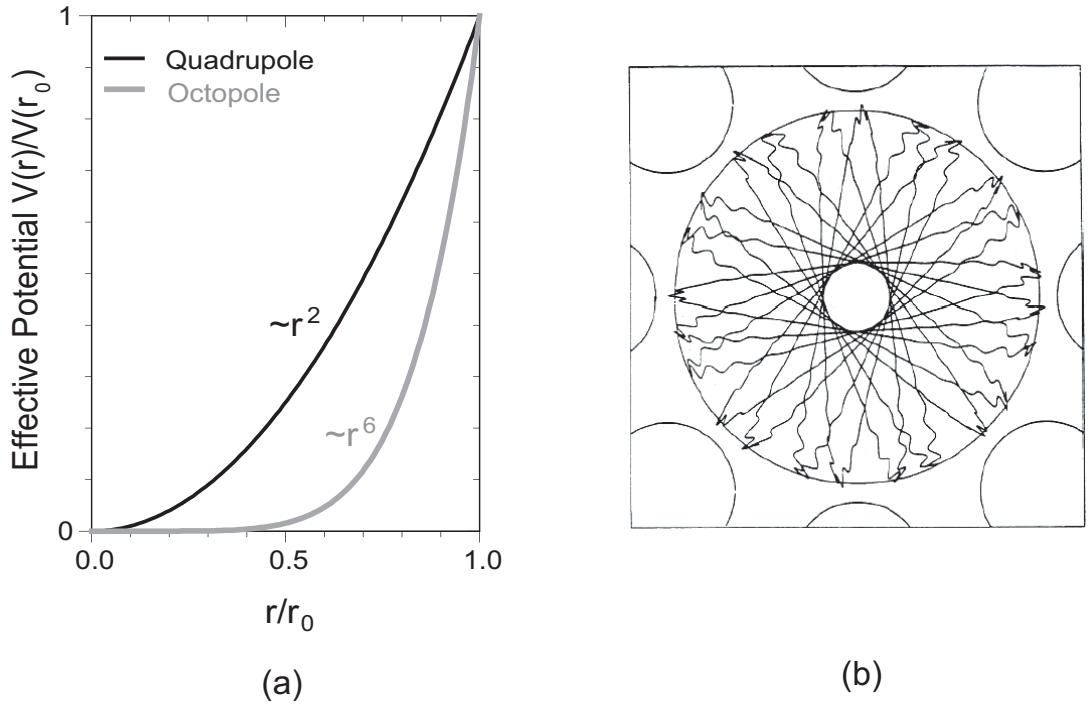

Figure 4.4: (a) Comparison between the effective potential of an octopole (black line) and of a quadrupole (grey line) ion trap as a function of the relative distance to the center of the trap. The effective potential for an octopole is directly proportional to r^6, while for a quadrupole the effective potential is directly proportional to r^2. (b) A typical trajectory of an ion inside an octopole ion trap, taken from Gerlich.[97] The picture is a transversal cross-section through an octopole, where the semicircles at the edge represent the rods of the octopole.

at the upper and lower part of the trap. During the measurements, a temperature difference of less than 5 K between the values indicated by the two thermocouples could be recorded.

The buffer gas and the reactive gases are introduced inside the octopole through a small teflon tube (1 mm diameter) and the gas pressure is measured with a capacitance manometer (Baratron, MKS, Model 627B). This type of manometer is widely used for measuring small gas pressures ($10^{-4} - 10^{-5}$ $Torr$), since the calibration is insensitive to the type of gas sample being measured. It was experimentally observed, that errors in the measured pressure values occur when the head of the manometer has a different temperature than the temperature of the volume to be measured and

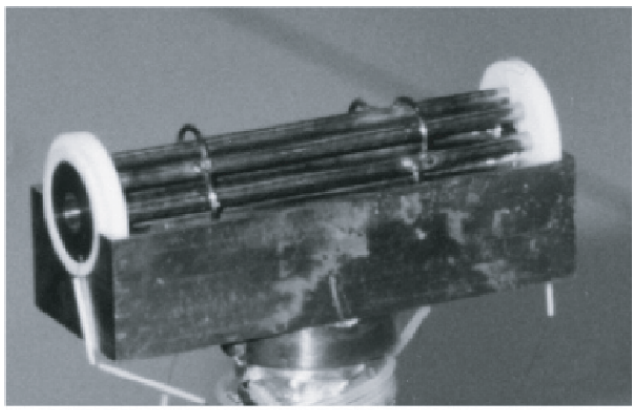

(a)

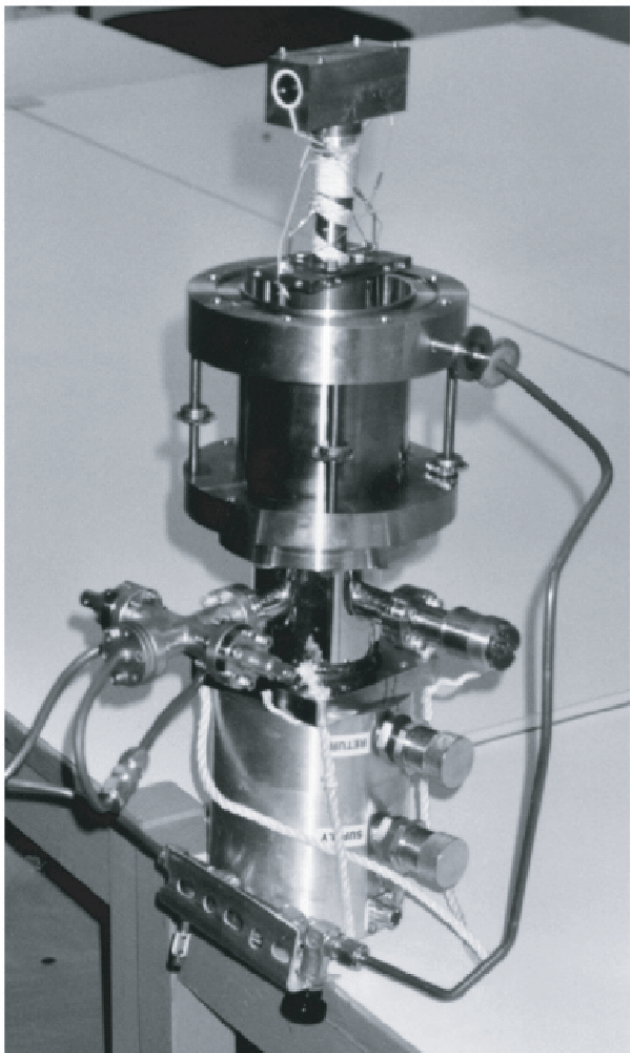

(b)

Figure 4.5: The octopole ion trap. (a) The octopole ion trap inside the gold plated housing. One can notice the octopole rods and the entrance and exit electrostatic lenses. (b) The octopole ion trap connected to the cryostat.

the diameter of the connection between the manometer and the pressure chamber is smaller than the mean free path of the gas atoms[d] at the cold end. This phenomenon is referred to as *"thermal transpiration"* and is caused by the apparition of a pressure gradient, resulting from the temperature gradient existing in the system. It was found that the correction term for the measured pressure is directly proportional to $\sqrt{T}$. Thus, the real pressure value inside the trap is:[98,99]

$$p_r = p_m \sqrt{\frac{T_t}{T_c}} \tag{4.7}$$

where p_r denotes the real pressure inside the octopole trap, p_m denotes the measured pressure, T_t represents the temperature of the ion trap and T_c represents the calibration temperature of the head of the manometer which has a value of 318 K for the experimental setup described in this work. For all experimental measurements presented in the following chapters the measured pressures p_m are indicated, while for the calculation of the reaction rate constants the correction factor for thermal transpiration is taken into account.

Another important aspect of the experimental setup is given by the thermalization of the clusters inside the ion trap. Since many physical and chemical properties of the clusters show a strong temperature dependence, it is very important to know the temperature of the ions prior to the chemical reaction. Through collisions between the clusters and buffer gas molecules inside the octopole ion trap, an energy transfer occurs and the clusters are cooled down to the noble gas temperature. In order to estimate the number of collisions with buffer gas atoms required to fully thermalize the clusters, a simple expression can be written for the cluster temperature after m collisions:[100]

$$T_c(m) = (T_c(0) - T_g)\left(1 - \frac{k}{3nk_B}\right)^m + T_g \tag{4.8}$$

where $T_c(m)$ denotes the cluster temperature after m collisions, $T_c(0)$ represents the initial cluster temperature, T_g denotes the buffer gas temperature, n denotes the number of atoms in the cluster and k represents the energy exchange parameter, which depends on the atomic mass of the buffer gas, the atomic mass of the cluster and interaction strengths. Molecular dynamics[100] and ergodic collision theory[e] (ECT)[101]

[d] In the case of helium atoms the mean free path for a gas pressure of 1 Pa and a temperature of 300 K has a value of about 3 cm.

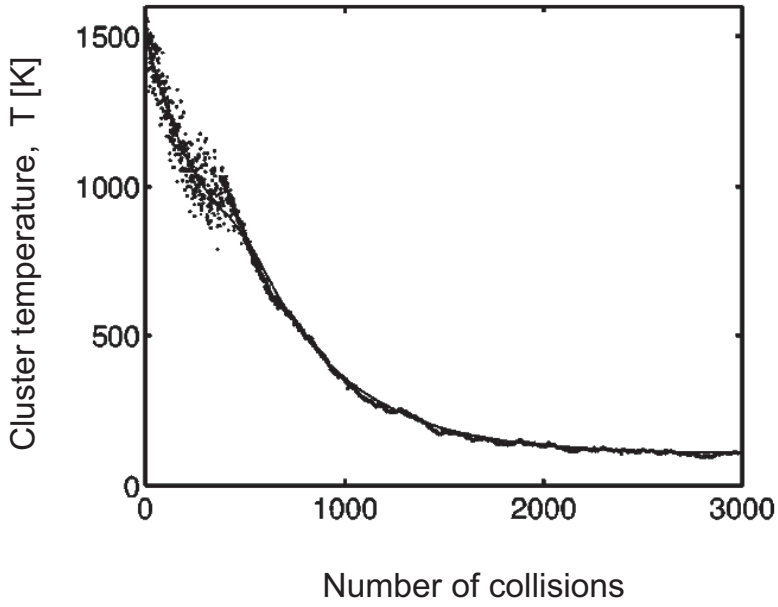

Figure 4.6: Thermalization of Pd_{13} cluster through collisions with helium atoms, taken from Westergren *et al.*[101] The initial cluster temperature has a value of 1500 K and the buffer gas temperature has a value of 100 K.

were applied to simulate the cooling of a metal cluster in noble gas environment. In Fig. 4.6, the cooling of a Pd_{13} cluster with an initial temperature of 1500 K in a helium atmosphere with a temperature of 100 K is shown. One can observe that about $2000 - 3000$ collisions are necessary to completely thermalize the clusters.

By considering equation 4.8, H. Heß simulated the cooling process of Ag_3 clusters in a helium atmosphere inside the octopole ion trap.[75] From these simulations, it was obtained that approximately 1000 collisions are necessary to thermalize the Ag_3 clusters. Under the experimental conditions for the measurements presented in this work, the thermalization requirement is fulfilled within a few milliseconds.[75]

In the process of collisional ion cooling inside an RF-ion trap, the field frequency, the geometry of the trap and the mass ratio between the ions and cooling atoms play an important role. Due to this, an efficient cooling requires: (*i*) high RF-frequencies, (*ii*) the mass of the buffer gas atoms should be small in comparison with the ion mass and (*iii*) the trap should have a large field-free region with steep confining walls, *i.e.*

[e]The ergodic collision theory assumes that after the collision process the colliding molecules are in microcanonical equilibrium with each other.

the number of the electrodes should be as large as possible.

In the following, the experimental procedure employed for measuring the reactivity of small noble metal clusters towards oxygen and carbon monoxide will be described in detail.

4.1.3 Measurement Procedure

A typical experiment for the study of the chemical reactivity of noble metal clusters begins with the production of the cluster beam. After the adjustment of the source, the quadrupoles Q_0, Q_1, Q_2 and the electrostatic lenses, the clusters are introduced inside the octopole ion trap. The cluster signal usually has an intensity of about 0.5 nA for Au_2^- measured on the rods of Q_2 with a picoampermeter (Keithley Instruments, Model 617). If necessary, a second thermalization of the clusters by using helium as buffer gas can be performed in the Q_2 quadrupole. Inside the octopole ion trap, the buffer gas is introduced ($p_{He,Ar} \cong 1\ Pa$) and following this, the reactive gases are added ($p_{gases} = 0.01\ Pa - 0.30\ Pa$). A cold trap filled with liquid nitrogen is used to clean the gases before entering the vacuum apparatus.

The operation of the ion trap in the filling, storing or extracting mode is controlled by using a LabView program (National Instruments, Version 5.1), developed for this purpose. Through a computer interface (Scientific Research Instruments, Model SR 245), the program commands two TTL-switches that change the voltages on the entrance and exit lenses of the octopole. During the filling time, the voltage on the entrance lens has a low negative value, allowing the clusters to enter the trap, while the voltage on the exit lens is high. The value of the entrance lens voltage is chosen so that the clusters only possess the minimal amount of kinetic energy that is necessary to just overcome the potential barrier of the electrostatic lens. Once entered in the octopole ion trap, the kinetic energy of the clusters is reduced through collisions with the buffer gas molecules so that their kinetic energy is not sufficient to allow the clusters to pass back over the entrance lens potential. In all the experiments presented here, the filling time was $t_{fill} = 100\ ms$. After the trap is filled, the voltage on the entrance lens is switched to a higher negative value. The trap is now closed and the clusters interact with the reactive gases during the reaction time $t_{reaction}$. Depending on the type of reaction, reactive gas pressure and temperature, the reaction

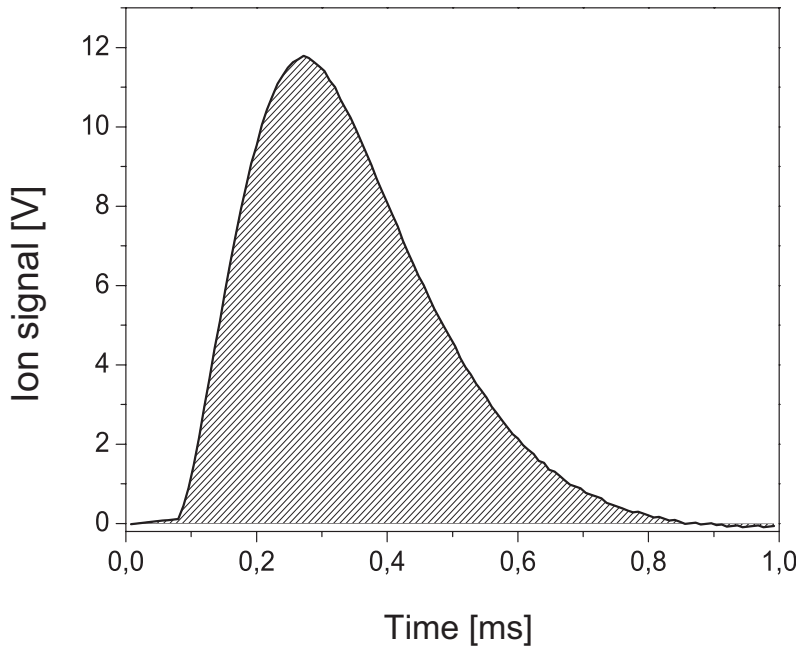

Figure 4.7: The averaged ion signal after 10 trap cycles measured with a LeCroy oscilloscope. The hatched area under the graph is directly proportional to the number of measured ions.

time can take on values between a few milliseconds and ten seconds. After a given reaction time, the voltage on the exit lens is switched to a positive value and all the reaction products are extracted into the last quadrupole mass spectrometer Q_3. The extraction time is fixed at $t_{extraction} = 40\ ms$ for all the experiments presented in this work. During the extraction process, all the ions are expelled so that after 40 ms the ion trap is empty and another cycle can begin. The voltage values for the entrance and exit lenses are chosen so that no further clusters can enter the trap during the reaction time, when both lenses are closed. The ion losses during the storage are less than 10% after 10 s reaction time. The trap is filled up to space charge limit, which amounts to approximately 7 pC[75] and an ion density of about $10^7\ ions/cm^3$ is used in every trap cycle. The ion density inside the trap is orders of magnitude smaller than the density of the buffer gas molecules, which is on the order of $10^{14}\ molecules/cm^3$ at a ion trap temperature of 300 K.

The ion signal is measured by using a channeltron detector placed close to a dynode. The polarity of the voltages applied on the detector depends on the charge

of the detected ions. At the end of the channeltron, the signal is collected and further amplified by using a fast amplifier (Femto, Model DLPCA-200). In the case of the negative ion detection, a capacitor isolates the high voltage region of the channeltron against the amplifier. The ion signal is then recorded with an oscilloscope (LeCroy, Model 9400 A). In Fig. 4.7, the averaged signal of a typical ion avalanche recorded with the oscilloscope is depicted. The ion avalanche presents an abrupt increase and a long decreasing tail as a function of time. The hatched area represents the integrated signal and is directly proportional to the measured ion intensity. The oscilloscope takes the spectra for 10 cycles of the ion trap, averages the spectra and sends the averaged signal to the computer. The computer program integrates the signal (the hatched area in Fig. 4.7), giving a value for the ion signal. This value represents a measurement point in the experimental reactivity spectra.

With this experimental arrangement, two types of measurements can be performed. *Mass spectra* can be recorded if the reaction time $t_{reaction}$ is kept constant and the mass of the reaction products is scanned with the quadrupole Q_3. When Q_3 is set to select a specific mass of a reaction educt or product and the reaction time is varied, *kinetic measurements* can be acquired. In this case, the time evolution of the concentration of a particular reaction product or educt is analyzed as a function of the reaction time. With this type of measurement, the kinetics of a reaction component can be monitored. The experimental measurements of the reactivity of small gold clusters towards oxygen and carbon monoxide will be shown in chapter 5.

4.2 Laser System

In this section, the femtosecond (fs) laser system utilized for measuring the dynamics of small noble metal clusters on an ultrashort time scale will be presented. Compared to previous fs-experiments,[75,76,93] a new laser system is employed for the measurements presented here, which allows the generation of 50 fs laser pulses after the amplification process. This laser system is presented in detail in the work of M. Krenz and only a short description will be given here.[102]

4.2.1 Generation and Characterization of a fs-Laser Pulse: Oscillator and Amplifier

The ultrashort laser pulses are generated with a femtosecond solid state laser, having a sapphire crystal doped with titanium ions as active medium (Ti:Sa). The Ti:Sa crystal has a broad absorption band situated in the blue-green spectral region ($450\ nm - 600\ nm$) with a maximum around $500\ nm$, which allows for the utilization of a green laser beam as pump. For the experimental setup presented here, a Nd:YVO_4 continuous wave (CW) laser (Spectra Physics, Model Millennia V), with an output wavelength of $\lambda = 532\ nm$ is used as a pump laser. The Ti:Sa crystal has a broad fluorescence in red-infrared spectral region ($680\ nm - 880\ nm$) with a maximum around $800\ nm$. The wavelength of the laser output can be tuned between $760\ nm$ and $840\ nm$. In the case of the experimental measurements described in this work, the central wavelength of the generated laser pulses was fixed at $\lambda = 805\ nm$. The fs-oscillator is a home-built laser,[102] following the plans of M. M. Murnane and H. C. Kapteyn.[103] A detailed view of the fs-oscillator is presented in Fig. 4.8, where the geometrical arrangement of the crystal, the prism pair and the folding mirror can be seen.

The generation of a fs-laser pulse is based on coupling the phase of different longitudinal modes within the laser cavity. This process is referred to as *mode-locking*. The spectral bandwidth of the laser pulse and therefore the pulse duration depend on the number of longitudinal modes, which are coupled in phase. For the fs-oscillator shown in Fig. 4.8, the mode-locking is obtained by using the nonlinear effect of self-focusing, which is known as *Kerr lens mode-locking*.[104] This process relies on the change of the refractive index of the active medium (Ti:Sa) in the presence of high field intensities, given by:

$$n(\omega) = n_0(\omega) + n_2(\omega) \cdot I(\omega) \tag{4.9}$$

where $n_0(\omega)$ is the fundamental refractive index of the active medium for a frequency ω, $n_2(\omega) \cdot I(\omega)$ represents the intensity dependent nonlinear contribution to the refractive index. Here, $I(\omega)$ denotes the high field intensity and $n(\omega)$ represents the total refractive index of the active medium. This change in the refractive index of the crystal leads to a change in the laser beam diameter and therefore to a focusing of the beam inside the crystal. The high field intensities, necessary for producing the

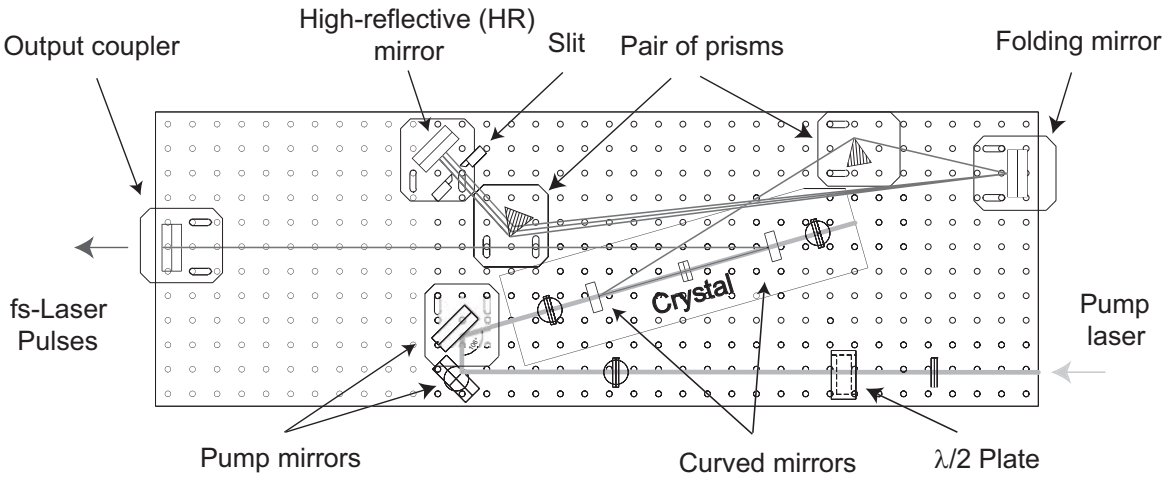

Figure 4.8: Detailed view of the fs-oscillator, adapted from Krenz.[102] The geometrical arrangement of the crystal, the prism pair and the folding mirror can be observed.

Kerr lens mode-locking are achieved by using the two curved mirrors placed near the Ti:Sa crystal, as shown in Fig. 4.8. By keeping the diameter of the pump beam small, the losses in the laser modes that are not coupled are high, while the losses in the locked modes are small, thus perpetuating the mode-locking process.

Due to the dispersion introduced by the propagation of the laser pulse in the laser cavity, the pulse will undergo a temporal broadening of the frequency spectrum. This means that different frequencies will have different propagation times. This would lead to a perturbation of the mode-locking process. In order to compensate the positive group velocity dispersion of the crystal (GVD > 0), other elements which possess a negative dispersion (GVD < 0) are introduced inside the fs-oscillator. Generally, an arrangement of four dispersive prisms is employed for the compensation of the pulse dispersion. Due to symmetry reasons, the four prisms can be replaced by an arrangement of two prisms and a high-reflective (HR) mirror, as it can be seen in Fig. 4.8. The mode-locking process is started by introducing a fluctuation of the laser intensity inside the fs-oscillator, which can be achieved by moving the prism that is positioned near the HR mirror. By mounting a slit in front of the high-reflective mirror (see Fig. 4.8), the central laser wavelength can be tuned between 760 nm and 840 nm.

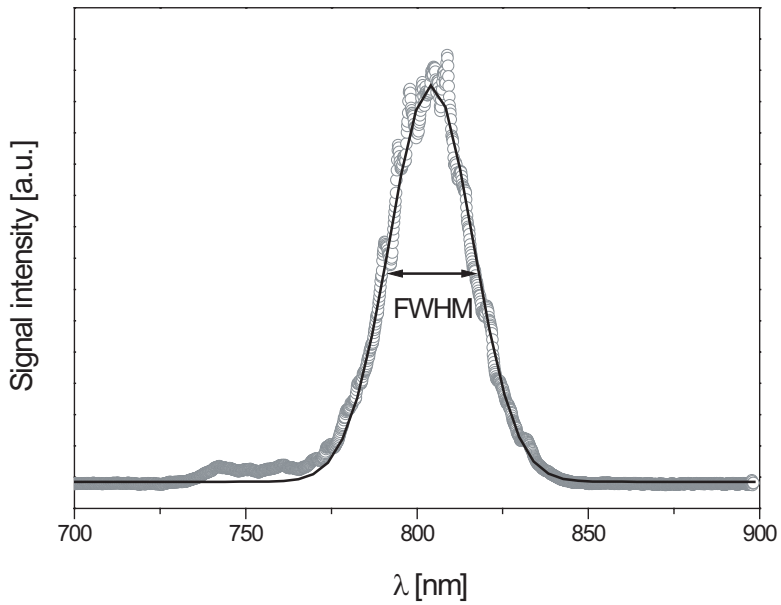

Figure 4.9: The spectrum of a fs-laser pulse generated by the oscillator (open grey circles). The gaussian function fit of the spectrum (black line) and the full width at half maximum (FWHM) are depicted on the graph. The FWHM has a value of about 30 nm.

With this experimental arrangement, ultrashort laser pulses with a duration of about 30 fs, at a central wavelength of $\lambda = 805\ nm$ can be generated. Fig. 4.9 shows a typical spectrum of the fs-laser pulses generated by the oscillator, measured with an optical fiber spectrometer (Avantes, Model AVS-S2000). The spectrometer allows the measurement of the wavelength between 600 nm and 900 nm and is utilized for the continuous monitoring of the laser pulses generated by the oscillator during the experiments.

The duration of the fs-laser pulse can be calculated from the spectral full width at half maximum (FWHM) (see Fig. 4.9) by using the following expression:[102]

$$\Delta\tau \geq K \cdot \frac{\lambda_0^2}{\Delta\lambda \cdot c_0} \tag{4.10}$$

where $\Delta\tau$ represents the pulse duration, λ_0 is the central wavelength of the laser pulse, $\Delta\lambda$ represents the measured FWHM, c_0 is the light velocity in vacuum and K is a factor which depends on the shape of the laser pulse. For a gaussian pulse, K

has a typical value of 0.441.

For a pump power of 5 W from the CW Nd:YVO_4 laser, the power of the fs-oscillator is about 500 mW at a repetition rate of 87 MHz, which represents a pulse energy of 6 nJ. By using a beam splitter (BS), approximately 30% from the outgoing laser beam is sent to a photodiode which is required for the trigger of the Pockels cell of the fs-amplifier system. From this 30%, an additional beam splitter sends 1% of the laser beam to the optical fiber spectrometer for monitoring the spectrum of the laser pulse. The remaining 70% of the laser beam generated by the fs-oscillator is used as a seed for the subsequent amplifier system, which will be described in detail in the following.

Since a direct amplification of the fs-seed pulses would lead to the damaging of the optical components due to the high peak intensities, the fs-laser pulses have to be stretched prior to amplification. This technique is known as *chirped pulse amplification*.[105] The stretching of the pulse refers to the generation of a time delay between the different frequency components of the laser pulse with respect to one another. In this way, a ps-pulse (30 $ps - 100$ ps) is obtained from a fs-laser pulse. The stretching of the laser pulse is achieved by using a specific arrangement of optical gratings.[102]

The multipass fs-amplifier is a commercially available system (Quantronix, Model Odin DQ), pumped by a Q-switched Nd:YLF laser (Quantronix, Model 527 DQ-1) that emits nanoseconds laser pulses at a wavelength of $\lambda = 527$ nm and a repetition rate of 1 KHz. The working principle of the multipass amplifier relies on the repetitive amplification of a laser pulse, which passes many times through the laser crystal. With every pass through the crystal, the stretched pulse depletes the population inversion generated by the green ns-pump pulse inside the crystal and thus, it is amplified. The fs-amplifier utilized for the experiments presented in this work has a Ti:Sa crystal as active medium and the laser pulse undergoes eight passes through the crystal. The geometry of the amplification stage is shown in Fig. 4.10. With this arrangement, an amplification of $2.5 \cdot 10^5$ in the intensity of the seed pulse can be obtained.[102] The synchronization in the timing of the fs-seed pulse and the ns-pump pulse is obtained by using a Pockels cell, which reduces the repetition rate of 87 MHz of the Ti:Sa oscillator to 1 KHz by picking only 1 pulse from 87000 arriving fs-pulses per second and this pulse is then amplified. After amplification, the pulses are passing through an

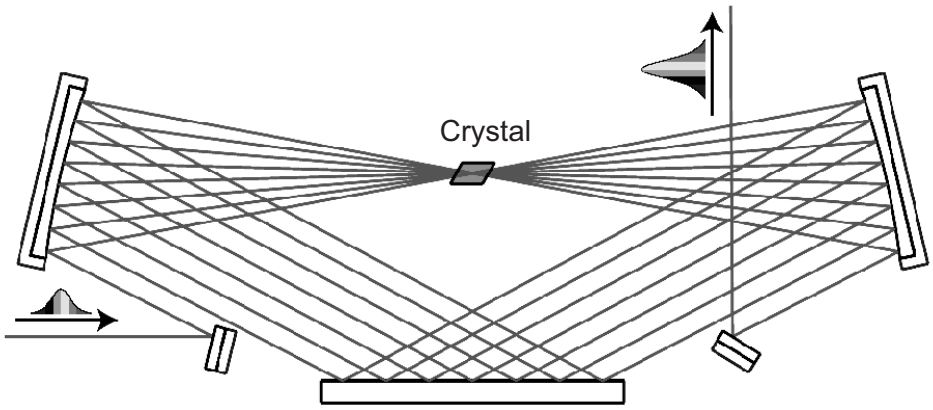

Figure 4.10: The geometry of the amplification stage inside the multipass amplifier where the eight passes through the Ti:Sa crystal are shown explicitly, adapted from Krenz.[102]

arrangement of optical gratings (compressor), where the inverse process of stretching is performed and the amplified ps-pulse is compressed back to a fs-pulse.

With this experimental setup, laser pulses with a minimum duration of about 50 fs, at a central wavelength of $\lambda = 810\ nm$ can be obtained after the amplification process. The change in the central wavelength of the laser pulse is referred to as *gain shifting*.[106] This process is a consequence of the fact that the red components of the laser pulse undergo a higher amplification than the blue components due to the amplifying profile in the Ti:Sa crystal. The power of the amplified laser beam has a value of approximately 1 W at a repetition rate of 1 KHz, which represents a pulse energy of 1 mJ for a pump power of the Nd:YLF laser of about 14 W. An autocorrelator (APE, Model PulsCheck) is employed for the measurements of the laser pulse duration.

For the investigation of the fs-dynamics of small noble metal clusters, it is important to have the possibility of tuning the wavelength of the employed laser pulses. This can be achieved by using an optical parametric amplifier (OPA) that allows the tuning of the wavelength from ultraviolet (UV) to infrared (IR) spectral region. The working principle of the optical parametric amplifier will be presented in detail in the next section.

4.2.2 Optical Parametric Amplifier

The process of tuning the wavelength of a laser beam is based on the principle of *frequency mixing*.[104] Frequency mixing can be obtained in anisotropic materials, that possess a high nonlinear second-order optical susceptibility ($\chi^{(2)} > 0$). In this type of materials, nonlinear processes such as *second harmonic generation* (SHG), *sum frequency generation* (SFG) or *difference frequency generation* (DFG) can be produced. The process of SHG implies that from two incoming photons with the same frequency ω, one photon with the frequency 2ω can be generated. In the case of SFG and DFG, two incoming photons having the frequencies ω_1 and ω_2 generate a third photon with the frequency ω_3 corresponding to the sum of the initial frequencies $\omega_3 = \omega_1 + \omega_2$ (SFG) or the frequency difference $\omega_3 = \omega_1 - \omega_2$ (DFG). For these processes to occur, the *phase-matching condition* must be fulfilled:[104]

$$\overrightarrow{k_1} + \overrightarrow{k_2} = \overrightarrow{k_3} + \Delta\overrightarrow{k} \tag{4.11}$$

where $\overrightarrow{k_1}$, $\overrightarrow{k_2}$ and $\overrightarrow{k_3}$ represent the wave vectors of the three photons and $\Delta\overrightarrow{k}$ represents the mismatch factor. For an efficient frequency conversion, the mismatch factor should be equal to zero ($|\Delta\overrightarrow{k}| = 0$). Generally, nonlinear crystals such as BBO (β-barium borate) or LBO (lithium triborate) are utilized for obtaining an efficient frequency mixing.

The working principle of an optical parametric amplifier relies on the process of difference frequency generation. In this case, a pump photon coming from an intense leaser beam with the frequency ω_p can mix inside a nonlinear crystal with an infrared photon produced from the quantum noise in the crystal, referred to as signal (ω_s) and generate another infrared photon, known as idler ($\omega_i = \omega_p - \omega_s$).[107,108] Thus, a broad infrared spectrum can be generated. The wavelength of the signal and idler can be tuned by changing the phase-matching angle of the nonlinear crystal. During the parametric amplification process, the pump, signal and idler interact with each other, leading to a reciprocal amplification.

For the experiments presented in chapter 6, two optical parametric amplifiers (TOPAS - Traveling Wave Optical Parametric Amplifier of Superfluorescence) are used. This type of optical parametric amplifier has a frequency conversion efficiency of up to 25 % from the incoming laser beam, with a four stage amplification configuration. Fig. 4.11 shows the geometry of the five passes of the laser beam through the

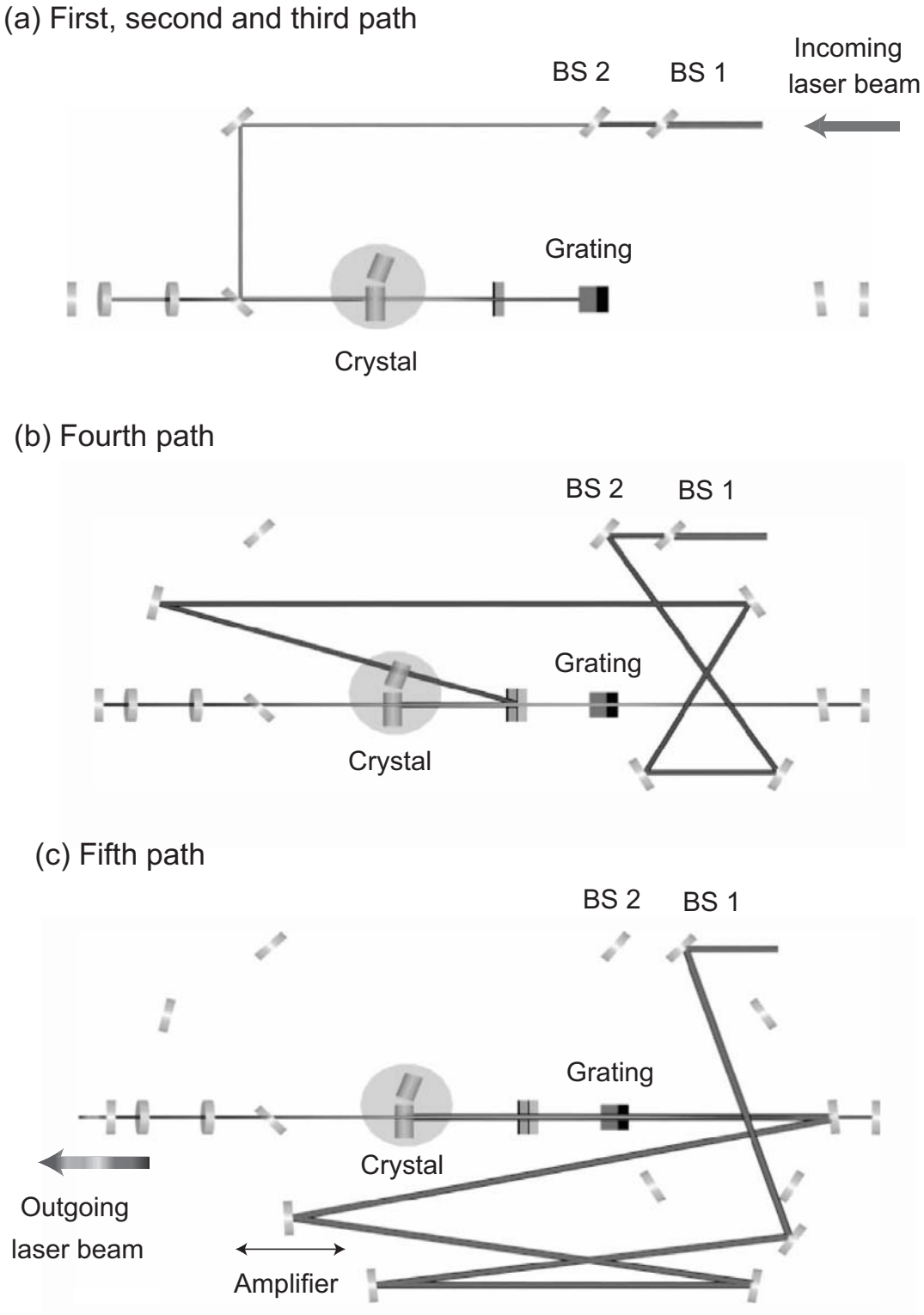

Figure 4.11: TOPAS: a schematic representation of the (a) first, second and third beam pass; (b) fourth pass; (c) fifth beam pass through the nonlinear crystal. The position of the crystal, optical grating and the beam splitters (BS 1, BS 2) is indicated on the figure, adapted from Krenz.[102]

crystal inside a TOPAS (Light Conversion, Model 4/800), where the position of the nonlinear crystal, optical grating and the two beam splitters (BS 1, BS 2) is indicated. In the first pass, 5 % of the incoming beam is separated by using the beam splitters BS 1 and BS 2, and it is utilized for producing the parametric superfluorescence inside the nonlinear crystal. In the second and third pass the generated IR superfluorescence signal (1200 $nm - 1600$ nm) is amplified by several orders of magnitude. The desired wavelength of the signal and idler is selected by the optical grating (see Fig. 4.11 (a)). In the fourth pass, another 5 % from the incoming laser beam are used to amplify the selected signal and idler wavelengths, as shown in Fig. 4.11 (b). The fifth pass utilizes the remaining 90 % of the incoming laser beam for the main parametric amplification of the signal and idler (see Fig. 4.11 (c)). Optionally, two mixers that contain nonlinear crystals can be mounted at the output of the TOPAS. In this way, the pump, signal and idler can be additionally mixed (sum-frequency and second harmonic) and a continuously tunable spectrum between 250 nm and 1200 nm can be obtained. Inside the TOPAS, the crystal, optical grating and mixers are mounted on rotation stages, which can be computer controlled by using the software WinTOPAS (Light Conversion, Version WinTOPAS 1/2). The wavelength of the laser pulse after the TOPAS is monitored by using an optical fiber spectrometer (Avantes, Model AVS-S2000), which has a broad spectral range from the ultraviolet to visible and near infrared (180 $nm - 880$ nm).

For the experimental measurements of the fs-dynamics of small noble metal clusters, the spectral region 300 $nm - 350$ nm of the TOPAS has been primarily used. The tuning of the wavelength for this spectral domain is achieved by the generation of the second harmonic of the second harmonic of signal (SH(SHS)). For a typical pump power of 600 mW at a wavelength of $\lambda = 810$ nm, the pulse energy of the outgoing laser beam is about 2 μJ for $\lambda = 320$ nm and 5 μJ for $\lambda = 350$ nm. The pump-probe setup and the measurement procedure utilized for the experiments presented in chapter 6 will be presented in the next section.

4.2.3 Pump-Probe Setup and Measurement Procedure

Fig. 4.12 shows the entire experimental setup, consisting of the laser system and the triple quadrupole mass spectrometer. From this figure, it can be seen that the laser beam is separated in two parts (pump and probe beam lines) after the multipass amplifier by using a beam splitter (BS). About 60 % are sent into the first optical parametric amplifier (TOPAS I) for the generation of the ultraviolet ($300\ nm - 350\ nm$) pump laser beam. The remaining 40 % are sent either to a second optical parametric amplifier (TOPAS II), which allows the wavelength variation of the probe pulse, or to a frequency doubling nonlinear crystal (BBO). For the pump-probe experiments presented in chapter 6, only one TOPAS was used for varying the wavelength of the pump pulse. For the probe pulse, a wavelength of $\lambda = 406\ nm$ was employed, that was obtained from the second harmonic generation in a BBO crystal (see Fig. 4.12). The 406 nm laser pulse is directed to a computer controlled delay stage (Physik Instrumente, Model C812), which introduces a delay time Δt between the pump and the probe pulses. With this method, time-dependent measurements of the fs-dynamics of small noble metal clusters can be carried out. As shown in Fig. 4.12, the two laser beams are brought together with the help of a dichroic mirror (DM) after the probe pulse passes through the delay stage. By using aluminium coated mirrors, the laser beams are directed inside the octopole ion trap. This represents the pump-probe setup for two-color measurements. In the case of one-color pump-probe experiments, when the pump and the probe pulses have the same wavelength, the splitting of the laser beam in pump and probe parts is performed after the second harmonic generation in the BBO crystal. The power of the laser pulses is measured on the laser table and these are the values that are indicated for the experiments presented in this work. Due to the high reflective losses caused by the four aluminium coated mirrors which guide the laser beams inside the octopole ion trap, the power of the laser beam just before entering the vacuum apparatus represents 50% from the initial value measured on the laser table.

The characterization of the laser pulses is performed *in situ*, in order to obtain exact information about the temporal length of the pulse after passing through all the optical components. By using a linear translator, a gold plate is introduced between the second quadrupole Q_2 and the octopole ion trap. The measurements procedure is based on the two-photon photoemission process, *i.e.* photoelectrons are emitted

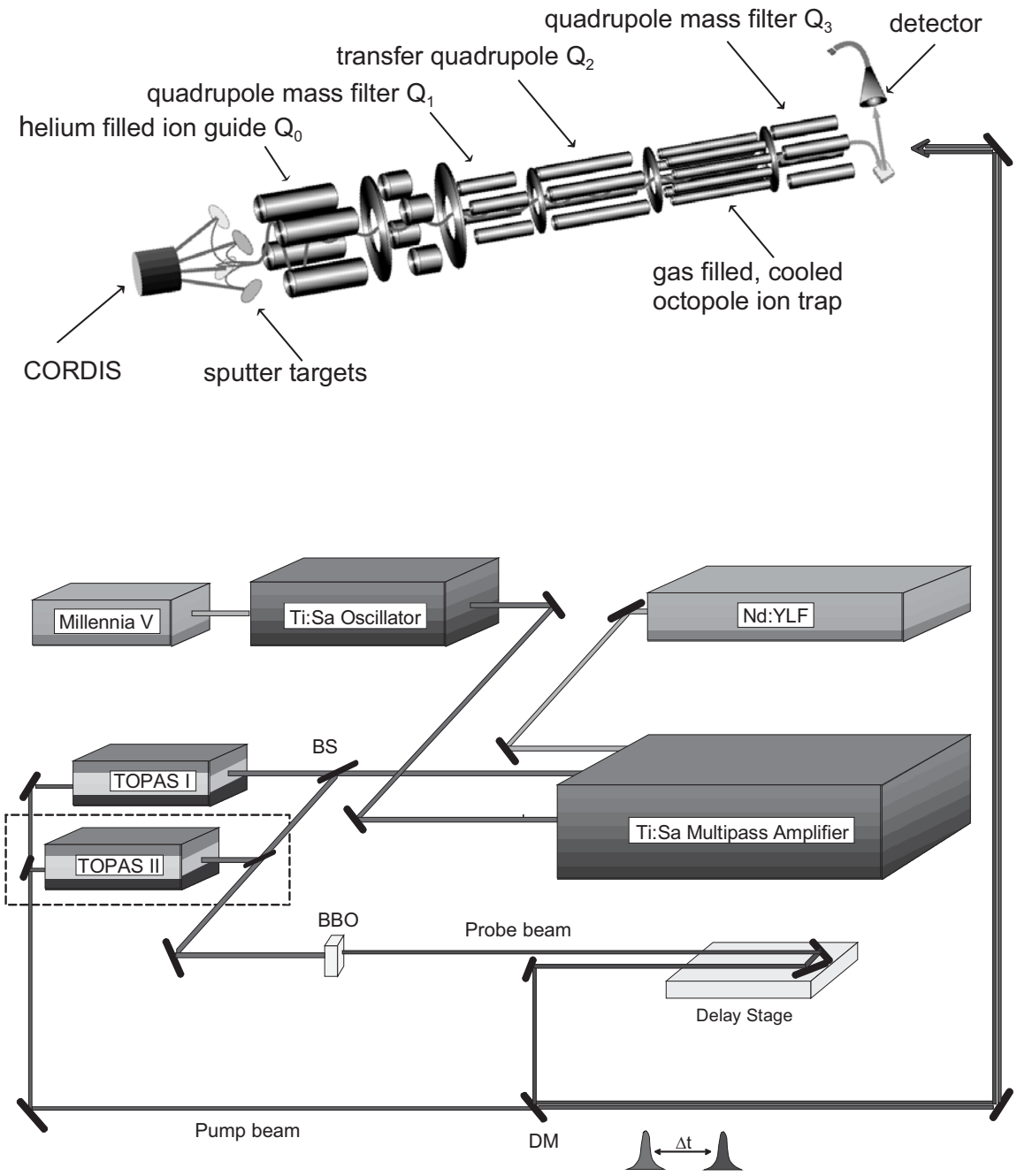

Figure 4.12: The experimental setup composed of the laser system and the triple quadrupole mass spectrometer. The second TOPAS (TOPAS II), which is shown in a dashed square, allows the wavelength variation of the probe pulse. For the experiments presented in chapter 6, only a frequency doubling BBO crystal was used for obtaining the probe pulse with a wavelength of $\lambda = 406\ nm$. The position of the beam splitter (BS) and the dichroic mirror (DM) is shown on the figure.

from the gold plate under the irradiation with the laser pulses. A picoampermeter (Keithley Instruments, Model 617) measures the current of the positive charges which remain on the gold plate as a function of the delay time between the two laser pulses. Since the gold plate has a work function[f] of 5.2 eV,[91] a single ultraviolet or blue photon which have energies between 3 eV and 4 eV are not sufficient for extracting photoelectrons from the gold plate. Therefore, it is necessary for both laser pulses to arrive simultaneously on the gold plate in order to extract photoelectrons. In this way, the crosscorrelation function[g] of the two laser pulses can be measured. This method is applied as well for determining the zero delay time[h] for the pump-probe fs-measurements. Any other metal (silver, copper, etc.) can be used as a photoelectron emitter. Gold presents the advantage of having excited states with a very short lifetime ($\sim$ 2 fs[109]) and due to this, the measurement of the duration of the laser pulse is not perturbed by the relaxation time of the hot electrons created with the first laser pulse. Another advantage of gold is that its surface does not oxidize and therefore the measurements of the temporal pulse length are not influenced by the formation of surface oxides which could lead to a change in the work function of the gold plate.

The intensity of the positive charge current measured on the gold plate is given by the autocorrelation function between the pump and the probe laser pulses:

$$I(\tau) = \int_{-\infty}^{\infty} |E(t) + E(t-\tau)|^2 dt \tag{4.12}$$

where $I(\tau)$ represents the measured current intensity, τ is the delay time between the two laser pulses, $E(t)$ and $E(t-\tau)$ represent the time-dependent profile of the electrical field of the pump and probe pulse, respectively. The correspondence between the full width at half maximum (FWHM) determined from the measured autocorrelation curve ($\Delta\tau$) and the FWHM of the laser pulse (Δt) is given by the expression:

$$\Delta t = \frac{\Delta\tau}{K} \tag{4.13}$$

where K represents the autocorrelation factor. For a gaussian shape of the laser pulses, K has a value of 1.414.

[f] The work function of a metal is defined as the energy difference between the vacuum level (E_{vac}) and the energy of the Fermi level (E_F).

[g] When the two laser pulses have the same wavelength, the autocorrelation function is obtained.

[h] The zero delay time represents the temporal superposition of the two laser pulses, *i.e.* the time when the pump and the probe laser pulses arrive simultaneously on the sample.

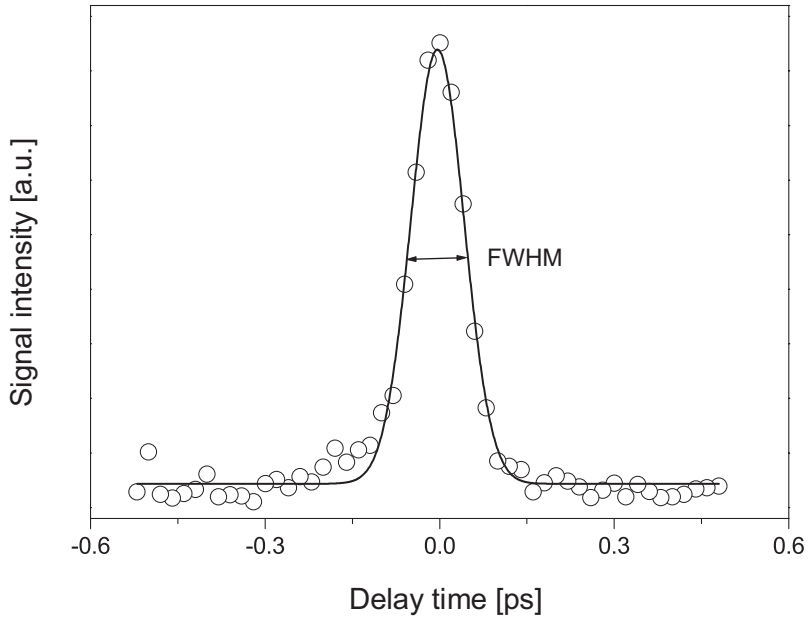

Figure 4.13: The autocorrelation trace of the pump and probe pulses as a function of the delay time between the two laser pulses measured on the gold plate. The open circles represent the experimental data and the solid line represents a gaussian fit of the measured signal. The experimental parameters are: $\lambda_{Pump} = \lambda_{Probe} = 406\ nm$, $P_{Pump} = P_{Probe} = 2.3\ mW$. The FWHM is shown on the figure and has a value of about 105 fs.

Fig. 4.13 shows the autocorrelation trace as a function of the delay time between the pump and the probe pulses measured on the gold plate for the pump and probe pulses with a wavelength of $\lambda_{Pump} = \lambda_{Probe} = 406\ nm$. The measured full width at half maximum (FWHM) for this autocorrelation trace has a value of about 105 fs. By using the expression 4.13, where $\Delta\tau = 105\ fs$ and assuming a gaussian shape for both laser pulses ($K = 1.414$), the duration of one laser pulse can be calculated. For the measurement presented in Fig. 4.13, the temporal length of the laser pulse is about 74 fs.

In Fig. 4.14, the crosscorrelation trace for the case of a two-color pump-probe experiment measured as a function of the delay time between the pump and the probe pulses is depicted. The solid line represents a gaussian fit to the experimental data. The wavelength of the pump pulse is $\lambda_{Pump} = 323\ nm$, while the wavelength of the probe pulse is $\lambda_{Probe} = 410\ nm$. As it can be seen from Fig. 4.14, the full width

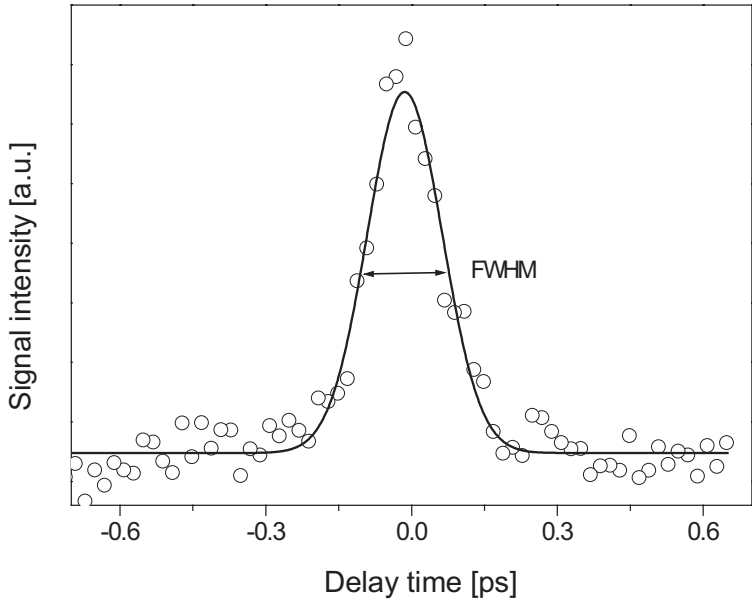

Figure 4.14: The crosscorrelation trace of the pump and probe pulses as a function of the delay time between the two laser pulses measured on the gold plate. The open circles represent the experimental data and the solid line represents a gaussian fit of the measured signal. The experimental parameters are: $\lambda_{Pump} = 323\ nm$, $\lambda_{Probe} = 410\ nm$, $P_{Pump} = 2.0\ mW$, $P_{Probe} = 10\ mW$. The FWHM is depicted on the figure and has a value of about 175 fs.

at half maximum is larger that in the case of a one-color pump-probe experiment and has a value of 175 fs. From measurements of the spectral profile of the pump and probe laser pulses, one can assume that both laser pulses have similar temporal lengths. By utilizing the expression 4.13 and considering a gaussian shape for both laser pulses, the duration of a laser pulse has a value of about 124 fs.

A typical measurement procedure starts with the production of the cluster beam, as described in section 4.1.3. After the alignment of the pump and probe beam, both laser beams are focused inside the octopole ion trap by using a lens with a focal distance of $f = 1\ m$, mounted in front of the vacuum apparatus. For all the experiments presented in this work, the intensity of the laser beam in the focus of the lens was about $10^{11}\ W/cm^2 - 10^{12}\ W/cm^2$. The temporal overlap (time zero) as well as the pulse length is detected by introducing the gold plate used for determining the crosscorrelation function in front of the octopole ion trap. For a typical negative-to-neutral-to-positive (NeNePo) measurement, the entrance lens of the octopole is

maintained open, *i.e.* the ion trap is filled continuously with negatively charged clusters, while the exit lens of the octopole is closed. The first laser pulse (pump pulse) detaches the electron from the negative clusters. After a given delay time, the second laser pulse (probe pulse) ionizes the neutral clusters. The positively charged clusters are expelled from the octopole ion trap and the current of the produced positive clusters is measured as a function of the delay time between the pump and the probe pulses by using a picoampermeter (Keithley Instruments, Model 617). The detection of positively charged clusters is performed as described in section 4.1.3. A LabView program (National Instruments, Version 5.1) averages three values of the measured cluster current for every value of the delay time. In order to reduce the experimental noise, each scan of the delay line is repeated for up to five times and the resulting spectra are averaged. The experimental measurements for the fs-dynamics of small noble metal clusters will be in detail presented in chapter 6.